UNIVERSIDAD DE CONCEPCIÓN

Centro de Investigación en Ingeniería Matemática (CI^{2}MA)

Numerical solution of a multi-class model for batch settling in water resource recovery facilities

Raimund Bürger, Stefan Diehl,
María Carmen Martí, Pep Mulet,
Ingmar Nopens, Elena Torfs,
Peter Vanrolleghem

PREPRINT 2016-39

SERIE DE PRE-PUBLICACIONES

NUMERICAL SOLUTION OF A MULTI-CLASS MODEL FOR BATCH SETTLING IN WATER RESOURCE RECOVERY FACILITIES

RAIMUND BÜRGER[A], STEFAN DIEHL[B], M. CARMEN MARTÍ[A,*], PEP MULET[C], INGMAR NOPENS[D], ELENA TORFS[E], AND PETER A. VANROLLEGHEM[E]

Abstract. In [E. Torfs et al., *Water Sci. Technol.*, in press] a new unified framework to model settling tanks in water resource recovery facilities was proposed providing a set of partial differential equations (PDEs) modelling different settling unit processes in wastewater treatment such as primary and secondary settling tanks (PSTs and SSTs). The extension to a multi-class framework to deal with the distributed properties of the settling particles leads to a system of nonlinear hyperbolic-parabolic PDEs whose solutions may contain really sharp transitions. This necessitates the use of a consistent and robust numerical method to obtain well-resolved and reliable approximations to the PDE solutions. The use of implicit-explicit Runge-Kutta (IMEX-RK) schemes, along with the weighted essentially non-oscillatory (WENO) shock-capturing technology for the discretization of the set of equations, is advocated in this work. The versatility of the proposed unified framework is demonstrated through a set of numerical examples for batch settling occuring in both PSTs and SSTs, along with the efficiency and reliability of the numerical scheme.

Keywords
multi-class kinematic flow model, wastewater treatment, convection-diffusion equation, implicit-explicit Runge-Kutta scheme, settling velocity distribution

1. Introduction

1.1. **Scope.** Several unit processes in water resource recovery facilities (WRRFs), formerly known as wastewater treatment plants (WTTPs), rely on settling as a separation method. These include primary and secondary settling tanks but also other processes such as sequencing batch reactors and grit chambers. According to the current state of the art, each of these unit processes is modelled in its own way and several models (ranging from very simplified to more fundamentally supported) are available for the various unit processes [2,6,25,26,32]. The reason for the choice of a particular model for each unit process lies in the variability of the settling suspensions (ranging, for example, from wastewater with approximately 0.1 g/l total suspended solids in PSTs to activated sludge with approximately 3 g/l total suspended solids in SSTs). Depending on the concentration of the suspension and its composition, different settling regimes occur. Settling can be either

Date: December 5, 2016.

*Corresponding author.

[a]CI^{2}MA and Departamento de Ingeniería Matemática, Facultad de Ciencias Físicas y Matemáticas, Universidad de Concepción, Casilla 160-C, Concepción, Chile. E-Mail: rburger@ing-mat.udec.cl, mmarti@ci2ma.udec.cl.

[b]Centre for Mathematical Sciences, Lund University, P.O. Box 118, S-221 00 Lund, Sweden. E-Mail: diehl@maths.lth.se.

[c]Departament de Matemàtiques, Universitat de València, Av. Vicent Andrés Estellés, s/n, E-46100 Burjassot, Spain, E-Mail: mulet@uv.es.

[d]BIOMATH, Department of Mathematical Modelling, Statistics and Bioinformatics, Ghent University, Coupure links 653, B-9000 Ghent, Belgium. E-Mail: ingmar.nopens@ugent.be.

[e]modelEAU, Département de génie civil et de génie des eaux, Université Laval, 1065 Av. de la Médecine, Quebec, QC G1V 0A6, Canada. E-Mail: elena.torfs.1@ulaval.ca, Peter.Vanrolleghem@gci.ulaval.ca.

discrete (at low concentrations where particles settle as individuals), hindered (in more concentrated suspensions where particles influence each other's settling and drag each other along) or compressive (at high concentrations where particles form a concentrated network and the stress developed by the network hampers further thickening), see [20].

Because the settling behaviour is so clearly influenced by the concentration of the suspension, settling models often describe the settling velocity as a function of concentration alone. However, the solid components in settling suspensions show a number of distributed properties that will also influence the settling behaviour. Examples of such distributed properties are size, shape, density or porosity. These distributed properties lead to a distributed settling velocity and changes in the distribution of these properties (for example due to different operational or environmental conditions) will lead to changes in the settling behaviour. Experimental evidence and examples of the effect of changes in size, shape and density distributions on the different settling regimes can be found in [34].

The influence of these distributed properties cannot be captured by a model that only considers the local concentration of the suspension. Advances in this domain have been made by Bachis et al. [2] who developed a model that considers distributions in settling velocity to describe discrete settling in PSTs. This concept was further extended to encompass also hindered and compression settling by Torfs et al. in [34] leading to a unified framework that is able to capture variability in distributed properties and their effect on all three settling regimes and that can thus model different settling unit processes. Implementation of this new framework requires appropriate numerics to ensure reliable and robust solutions. This is the focus of the current work.

1.2. **Related work.** From the mathematical point of view, the extension to a multi-class scenario leads us to a system of non-linear convection-diffusion equations of the type

$$\frac{\partial \boldsymbol{X}}{\partial t} + \frac{\partial \boldsymbol{f}(\boldsymbol{X})}{\partial z} = \frac{\partial}{\partial z}\left(\boldsymbol{B}(\boldsymbol{X})\frac{\partial \boldsymbol{X}}{\partial z}\right), \tag{1.1}$$

where $\boldsymbol{X} = (X_1, \ldots, X_N)^{\mathrm{T}}$ is the sought solution depending on the spatial position z and time t, $X_i = X_i(z,t)$ the concentration of the class i, $i = 1, \ldots, N$, where N is the number of classes considered, $\boldsymbol{f}(\boldsymbol{X}) = (f_1(\boldsymbol{X}), \ldots, f_N(\boldsymbol{X}))$ is a vector of convective flux density functions modelling the settling of the sludge and $\boldsymbol{B}(\boldsymbol{X})$ is a given $N \times N$ matrix expressing the diffusive correction, in this case, the solids compressibility. Other possible phenomena arising in continuously operated units such as advection (bulk movement of the suspension) and dispersion, are not considered in this work. Such effects will, however, not change the principal mathematical structure of (1.1). This system has to be supplied with initial and boundary conditions.

It is well known that (1.1) is a degenerate parabolic system. When compressibility effects are neglected, $\boldsymbol{B}(\boldsymbol{X}) = \boldsymbol{0}$, the settling effects are dominant and (1.1) is first-order hyperbolic, implying that discontinuities or sharp gradients are expected to develop. This property calls for specific techniques for the numerical simulations. High resolution shock-capturing finite difference weighted essentially non-oscillatory (WENO) schemes have been extensively used for the numerical treatment of hyperbolic one-dimensional multi-species flow models in recent years, especially in the area of polydisperse sedimentation of suspensions [7,8,12,24] and multi-class vehicular traffic [18,37,38]. These schemes combine an explicit time discretization [29, 30] with a high-order procedure for the spatial discretization of the convective term $\partial \boldsymbol{f}(\boldsymbol{X})/\partial z$, involving the use of the characteristic information of the system [19] and the WENO reconstruction technique [22, 23, 28]. Such sophisticated techniques ensure obtaining precise numerical approximations, accurately resolving the shocks arising and avoiding the spurious oscillations that otherwise often appear.

When diffusion terms become nonzero and the system (1.1) becomes parabolic, the stability condition defined in the hyperbolic case changes into a restrictive condition that diminishes the time step size dramatically, making the use of explicit schemes really inefficient, at least for the time discretization of the diffusive part. As the implicit treatment of the convective term is complicated, because of the nonlinear scheme with possibly discontinuous derivatives used for its spatial discretization, implicit-explicit (IMEX) schemes [1] emerge as an interesting alternative in this context, combining an explicit treatment for the time discretization of the convective terms with an implicit treatment of the diffusive ones. See also [16] for a discussion of this point.

The IMEX framework has been applied to extend the work done with high-resolution shock capturing schemes for hyperbolic systems to hyperbolic-parabolic systems in several areas: polydisperse sedimentation of suspensions [4, 5], multi-class vehicular traffic [4, 10], sedimentation in porous media [17, 21] among others and has been proven to be more efficient than explicit schemes in most of them.

1.3. **Outline of the paper.** In Section 2, we derive the model equations for the multi-class concentration-driven model for the treatment of wastewater first introduced in [34], detailing the simplifications and definitions for the constitutive functions considered in this work. In Section 3 we briefly review the numerical technique that we apply, paying attention to the spatial and temporal discretizations. In Section 4 we show numerically that the results obtained by the multi-class concentration-driven model proposed in [34] are consistent with those obtained by the reference model, the Bürger-Diehl model [6] ("BD model" henceforth). Within the multi-class model the settling behaviour does not only depend on the total initial concentration but also on the settling velocity distributions and the initial concentrations of the classes. It could be seen that the proposed numerical technique provides a robust and efficient tool to numerically solve this system of PDEs when applied to different unit processes. Finally, in Section 5 we present some conclusions.

2. Mathematical model

2.1. **Balance equations.** In [34], a unified description for the settling processes taking place in both PSTs and SSTs was proposed as an extension of the existing BD framework for SSTs [6]. Building on the idea that the distributed properties of the sludge can be captured by dividing the total sludge concentration into a number of particle classes, based on settling velocity distributions in this case, a system of conservation PDEs modelling the changes in concentration for all classes is introduced in [34]. This system is of the form

$$\frac{\partial X_i}{\partial t} = -\frac{\partial}{\partial z} F_i\left(X, \frac{\partial X}{\partial z}, X_i, z, t\right) + \frac{Q_{\mathrm{f}}(t) X_{\mathrm{f},i}(t)}{A}\delta(z) + r_i(Q_{\mathrm{f}}, X_i, X, C_{\mathrm{chem}}), \quad i = 1, \ldots, N, \quad (2.1)$$

where $X_i = X_i(z,t)$ is the concentration of particle class i, depending on depth z and time t, X is the total sludge concentration defined as the sum of the concentrations of all classes, $X = X_1 + \cdots + X_N$, F_i is the flux density function for class i, the source term with the delta function $\delta(z)$ models the incoming feed flow at the feed inlet, with Q_{f} the incoming feed flow rate, $X_{\mathrm{f},i}$ the concentration of class i in the feed flow, and A the constant cross-sectional area. The reaction terms $r_i(Q_{\mathrm{f}}, X_i, X, C_{\mathrm{chem}})$ describe flocculation/break-up processes that depend mainly on the incoming flow rate $Q_{\mathrm{f}}(t)$ but can also be influenced by the presence of chemicals represented by C_{chem}.

An important novelty of the model presented in [34] is a distributed flux function that describes distributed settling behaviour over the entire concentration interval (going from discrete settling at very dilute conditions to hindered and compression settling at more concentrated states).

We consider here a batch sedimentation case where the focus is on the settling flux and neither bulk flows nor incoming feed flow or reactions between classes are considered. Equation (2.1) can

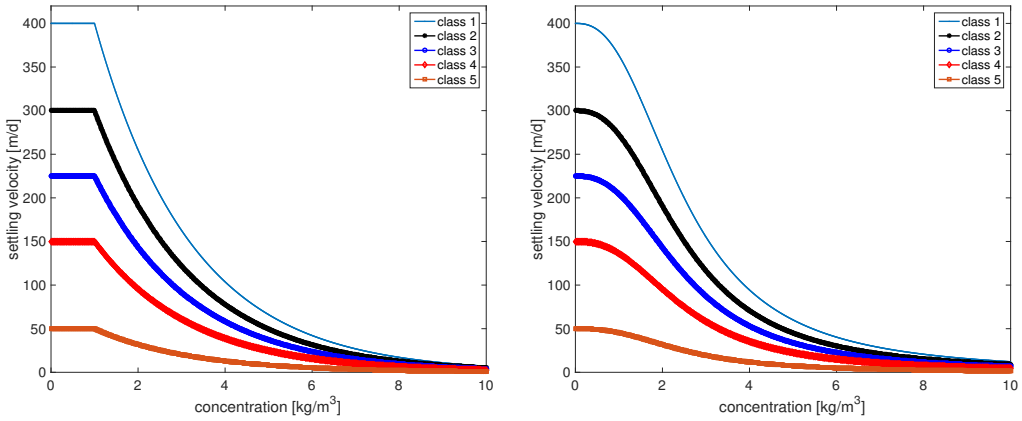

FIGURE 1. Settling velocities in function of concentration for different classes computed using both Vesilind hindered settling function [36] (left) and the rational function by Diehl [15] (right).

then be simplified and rewritten as follows:

$$\frac{\partial X_i}{\partial t} = -\frac{\partial}{\partial z} F_i\left(X, \frac{\partial X}{\partial z}, X_i, z, t\right), \quad i = 1, \ldots, N, \tag{2.2}$$

where the flux functions F_i are defined by

$$F_i\left(X, \frac{\partial X}{\partial z}, X_i, z, t\right) = \left(v_{\mathrm{dhs},i}(X) - \frac{d_{\mathrm{comp},i}(X)}{X}\frac{\partial X}{\partial z}\right) X_i, \quad i = 1, \ldots, N.$$

2.2. **Constitutive functions.** The following "discrete-hindered settling" velocity function that models both the distributed dynamics for discrete settling and the decreasing distributed behaviour during hindered settling, was proposed in [34]:

$$v_{\mathrm{dhs},i}(X) = \begin{cases} v_{0,i} & \text{for } X < X_{\mathrm{trans}}, \\ v_{0,i} v(X - X_{\mathrm{trans}}) & \text{for } X \geq X_{\mathrm{trans}}, \end{cases} \quad i = 1, \ldots, N. \tag{2.3}$$

The parameter $X_{\mathrm{trans}} \geq 0$ represents the transition concentration between discrete and hindered settling, $v_{0,i}$ is the maximum discrete settling velocity of phase i and $v(X)$ is given by a hindered settling function, for example by the expression

$$v(X) = \mathrm{e}^{-r_{\mathrm{V}} X}, \quad r_{\mathrm{V}} > 0 \tag{2.4}$$

due to Vesilind [36]. At concentrations $X < X_{\mathrm{trans}}$, the settling behaviour in each class i is governed by its discrete settling velocity $v_{0,i}$ while when the concentration increases and exceeds X_{trans}, the settling velocity decreases as the particles start to hinder each other's settling behaviour. Discrete settling is modelled by hindered settling functions satisfying $v'(0) = 0$. Hence, if this is already satisfied, e.g. by the rational function by Diehl [15], then a smooth transition between discrete and hindered settling is obtained without the parameter X_{trans}. An example of settling velocities computed using both Vesilind's and Diehl's hindered settling function can be seen in Figure 1.

The effect of sediment compressibility is traditionally modeled by a function d_{comp} depending on the total concentration that satisfies

$$d_{\text{comp}}(X)\begin{cases}=0 & \text{for } 0\le X\le X_{\text{crit}},\\ >0 & \text{for } X>X_{\text{crit}},\end{cases} \tag{2.5}$$

where X_{crit} is a critical concentration (defined below in (2.8)) at which the solid particles touch each other and start to form a porous network [14, 27]. The functional form of $d_{\text{comp},i}$, for $i=1,\dots,N$ can be defined by

$$d_{\text{comp},i}(X)=v_{\text{dhs},i}(X)\frac{\rho_X\sigma_{\text{e}}'(X)}{g(\rho_X-\rho_L)}, \tag{2.6}$$

where ρ_X and ρ_L are the solid and liquid mass densities respectively, g is the acceleration of gravity, and $\sigma_{\text{e}}'(X):=\mathrm{d}\sigma_{\text{e}}(X)/\mathrm{d}X$ is the derivative of the so-called effective solid stress function $\sigma_{\text{e}}=\sigma_{\text{e}}(X)$. This function is assumed to satisfy

$$\sigma_{\text{e}}'(X)\begin{cases}=0 & \text{for } 0\le X\le X_{\text{crit}},\\ >0 & \text{for } X>X_{\text{crit}},\end{cases}$$

which ensures that $d_{\text{comp},i}$ indeed has the property (2.5) for each $i=1,\dots,N$.

We can rewrite (2.2) as

$$\frac{\partial X_i}{\partial t}+\frac{\partial}{\partial z}\left(v_{\text{dhs},i}(X)X_i\right)=\frac{\partial}{\partial z}\left(\frac{d_{\text{comp},i}(X)}{X}X_i\frac{\partial X}{\partial z}\right),\quad i=1,\dots,N, \tag{2.7}$$

obtaining a system of convection-diffusion equations written in the same fashion as (1.1) with the flux density functions given by

$$f_i(\boldsymbol{X})=v_{\text{dhs},i}(X)X_i,\quad i=1,\dots,N,$$

and the diffusion matrix $\boldsymbol{B}(\boldsymbol{X})=(B_{ij}(\boldsymbol{X}))_{i,j=1,\dots,N}$, where

$$B_{ij}(\boldsymbol{X})=\frac{d_{\text{comp},i}(X)}{X}X_i,\quad i,j=1,\dots,N,$$

with the functions $v_{\text{dhs},i}(X)$ and $d_{\text{comp},i}(X)$ defined by (2.3) and (2.6), respectively.

2.3. **Mathematical properties of the governing model.** As the functions $v_{\text{dhs},i}(X)$ depend only on X, applying the secular equation analysis performed in [19], we can establish the hyperbolicity of the system, when $\boldsymbol{B}(\boldsymbol{X})=\boldsymbol{0}$, and that the eigenvalues of the Jacobian matrix of the system interlace with the velocities $v_{\text{dhs},i}$ [19]. This property is a key tool for the application of high resolution shock-capturing WENO schemes to numerically solve those systems. With respect to the diffusion matrix, when $\boldsymbol{B}(\boldsymbol{X})\neq\boldsymbol{0}$, it is a rank-one matrix, with $N-1$ zero eigenvalues and a non-zero eigenvalue $\sum_i d_{\text{comp},i}X_i/X>0$, for $X>X_{\text{crit}}$.

The specific concentration above which the sludge forms a compressible network has been shown to depend on the composition of the suspension [14,34]. Therefore, in [34] it is proposed to account for polydispersity in the definition of X_{crit} as follows: assume that each particle class i is associated with an individual critical density $X_{\text{crit},i}$, which may represent, for instance, the critical concentration in case a monodisperse sample of this class was settling. Then if $\boldsymbol{X}_{\text{crit}}:=(X_{\text{crit},1},\dots,X_{\text{crit},N})^{\text{T}}$, the total critical concentration can be defined as the following convex combination of the critical

concentrations of the classes:

$$X_{\mathrm{crit}} := \mathcal{X}_{\mathrm{crit}}(\boldsymbol{X}) := \begin{cases} \max\{X_{\mathrm{crit},1}, \dots, X_{\mathrm{crit},N}\} & \text{if } X = 0, \\ \displaystyle\sum_{i=1}^{N} \frac{X_i}{X} X_{\mathrm{crit},i} = \frac{1}{X} \boldsymbol{X}^{\mathrm{T}} \boldsymbol{X}_{\mathrm{crit}} & \text{if } X > 0. \end{cases} \tag{2.8}$$

Of particular interest is the critical manifold

$$\mathcal{M}_{\mathrm{crit}} := \{\boldsymbol{X} \in \mathbb{R}^N : X_1, \dots, X_N \geq 0, X = \mathcal{X}_{\mathrm{crit}}(\boldsymbol{X})\},$$

with $X = X_1 + \cdots + X_N$, which separates the phase space into two disjoint regions where the PDE system is hyperbolic and parabolic, respectively. By (2.8) we have $\boldsymbol{X} \in \mathcal{M}_{\mathrm{crit}}$ if and only if $J(\boldsymbol{X}) = 0$ and $\boldsymbol{X} \neq \boldsymbol{0}$, where

$$J(\boldsymbol{X}) := X^2 - \boldsymbol{X}^{\mathrm{T}} \boldsymbol{X}_{\mathrm{crit}}. \tag{2.9}$$

Clearly, $J(\boldsymbol{X}) < 0$ for small $|\boldsymbol{X}| > 0$, $\boldsymbol{X} \geq \boldsymbol{0}$, and $J(\boldsymbol{X}) \leq 0$ and $J(\boldsymbol{X}) > 0$ correspond to the regions where $d_{\mathrm{comp},i}(X) = 0$ and $d_{\mathrm{comp},i}(X) > 0$, respectively.

To illustrate that $\mathcal{M}_{\mathrm{crit}}$ separates a subregion of $\{\boldsymbol{X} \in \mathbb{R}^N : X_1, \dots, X_N \geq 0\}$, that is close to the origin from another region that is farther away, let $\boldsymbol{e} = (1, \dots, 1)^{\mathrm{T}}$, so that (2.9) can be written as $J(\boldsymbol{X}) = \boldsymbol{X}^{\mathrm{T}} \boldsymbol{e}\boldsymbol{e}^{\mathrm{T}} \boldsymbol{X} - \boldsymbol{X}^{\mathrm{T}} \boldsymbol{X}_{\mathrm{crit}}$. This is a quadratic form with the Hessian matrix $2\boldsymbol{e}\boldsymbol{e}^{\mathrm{T}}$, which is positive semidefinite. Hence J is a convex function and the set $K := \{\boldsymbol{X} \in \mathbb{R}^N : \boldsymbol{X} \geq \boldsymbol{0}, J(\boldsymbol{X}) \leq 0\}$ is convex by standard arguments. (If $\boldsymbol{X}, \boldsymbol{Y} \in K$, $0 < a < 1$ and $\boldsymbol{Z} := a\boldsymbol{X} + (1-a)\boldsymbol{Y}$, then it follows that $\boldsymbol{Z} \geq \boldsymbol{0}$ and $J(\boldsymbol{Z}) = J(a\boldsymbol{X} + (1-a)\boldsymbol{Y}) \leq aJ(\boldsymbol{X}) + (1-a)J(\boldsymbol{Y}) \leq 0$; hence $\boldsymbol{Z} \in K$.)

To visualize this manifold, we consider $N = 2$. From $J(\boldsymbol{X}) = 0$, we have that

$$Y_1 = -Y_2 + \frac{r}{2} + \sqrt{Y_2(1-r) + \frac{r^2}{4}}, \tag{2.10}$$

where $Y_i := X_i / X_{\mathrm{crit},2}$, $i = 1, 2$ and $r := X_{\mathrm{crit},1} / X_{\mathrm{crit},2}$. Consequently, the only relevant parameter is $0 \leq r \leq 1$. Figure 2 shows the corresponding critical manifolds, that is, solutions of (2.10).

3. Numerical method

In order to apply IMEX schemes to numerically compute accurate approximations to the solution of this convection-diffusion system of equations, first of all we define a semi-spatial discretization of the system setting a computational mesh on the interval $[0, L]$, with L the height of the vessel, by defining the grid points $z_j = (j - \frac{1}{2})\Delta z$ for $j = 1, \dots, M$ with $\Delta z = L/M$ the uniform grid spacing, $\Delta z = z_{j+1} - z_j$ for $j = 1, \dots, M$.

3.1. Spatial discretization.

Following the spatial discretization proposed in [10], we can discretize (2.7) in space as

$$\frac{\mathrm{d}X_{i,j}(t)}{\mathrm{d}t} := -\frac{1}{\Delta z} \Delta^- f_{i,j+1/2} + \frac{1}{\Delta z} \Delta^- g_{i,j+1/2}, \quad i = 1, \dots, N, \quad j = 1, \dots, M,$$

where $\Delta^- g_{l,k} = g_{l,k} - g_{l,k-1}$, the first term is the discretization of the convective term $\partial \boldsymbol{f}(\boldsymbol{X})/\partial z$ and the second part is the discretization of the diffusive term $(\partial/\partial z)(\boldsymbol{B}(\boldsymbol{X})\partial \boldsymbol{X}/\partial z)$.

For the discretization of the convective term we utilize a component-wise fifth-order WENO (WENO5) approximation [7, 37]. Component-wise finite differences WENO5 schemes compute the numerical fluxes $f_{i,j+1/2} \approx f_i(z_{j+1/2}, t)$ at the mesh mid-points $z_{j+1/2}$ as follows:

$$f_{i,j+1/2} = \mathcal{R}^+\big(f_i^+(X_{j-2}), \dots, f_i^+(X_{j+2}), z_{j+1/2}\big) + \mathcal{R}^-\big(f_i^-(X_{j-1}), \dots, f_i^-(X_{j+3}), z_{j+1/2}\big),$$

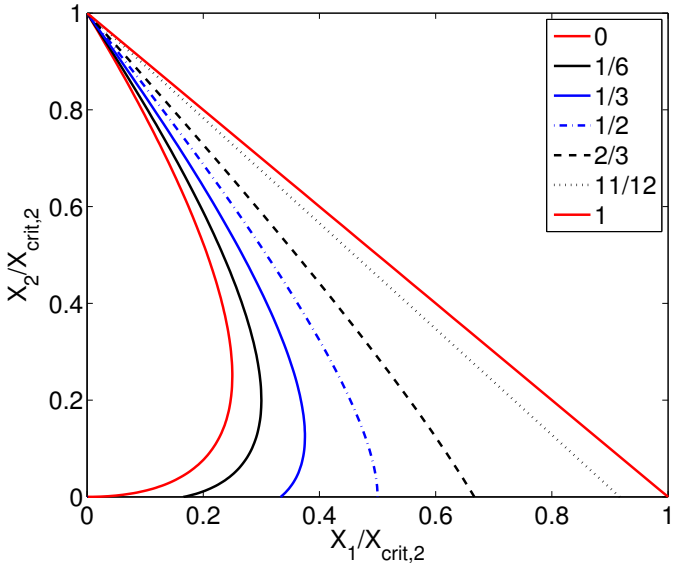

FIGURE 2. Critical manifolds $\mathcal{M}_{\text{crit}}$ for $r = X_{\text{crit},1}/X_{\text{crit},2} = 0, 1/6, 1/3, \ldots, 1$ calculated from (2.10). In each case, the region enclosed by $\mathcal{M}_{\text{crit}}$ and the X_1- and X_2-axes corresponds to $J(\boldsymbol{X}) \leq 0$, that is, to $d_{\text{comp}} = 0$, hence only discrete or hindered settling are present.

where X denotes the total solids concentration, $\mathcal{R}^{\pm}$ denotes the upwind-biased WENO5 reconstruction procedure and the functions $f_i^{\pm} = \frac{1}{2}(f_i \pm \alpha X_i)$ define a global Lax-Friedrichs flux splitting for each $i = 1, \ldots, N$. The numerical viscosity α, defined as a proper upper bound for characteristic velocities in the system being solved, can be numerically computed using the interlacing property [19]. For more detailed information about those schemes, see [22, 23, 28–30] and the references therein.

For the discretization of the diffusive part we define an approximate diffusive flux at $z_{j+1/2}$, that is

$$\boldsymbol{g}_{j+1/2} \approx \boldsymbol{B}(\boldsymbol{X}) \frac{\partial \boldsymbol{X}}{\partial z}\bigg|_{z=z_{j+1/2}}, \quad \boldsymbol{g}_{j+1/2} = (g_{1,j+1/2}, \ldots, g_{N,j+1/2})^{\mathrm{T}},$$

as follows:

$$\boldsymbol{g}_{j+1/2} := \frac{1}{2\Delta z}\big(\boldsymbol{B}(\boldsymbol{X}_{j+1}) + \boldsymbol{B}(\boldsymbol{X}_j)\big)\Delta^{-}\boldsymbol{X}_{j+1}, \quad j = 1, \ldots, M,$$

which gives a second-order approximation for the diffusive term of the form

$$\frac{1}{\Delta z}\Delta^{-}\boldsymbol{g}_{j+\frac{1}{2}} := \frac{1}{2\Delta z^2}\Big(\big(\boldsymbol{B}(\boldsymbol{X}_{j+1}) + \boldsymbol{B}(\boldsymbol{X}_j)\big)\boldsymbol{X}_{j+1} - \big(\boldsymbol{B}(\boldsymbol{X}_{j+1}) + 2\boldsymbol{B}(\boldsymbol{X}_j) + \boldsymbol{B}(\boldsymbol{X}_{j-1})\big)\boldsymbol{X}_j + \big(\boldsymbol{B}(\boldsymbol{X}_j) + \boldsymbol{B}(\boldsymbol{X}_{j-1})\big)\boldsymbol{X}_{j-1}\Big), \quad j = 2, \ldots, M-1.$$

For $j = 1$ and $j = M$ this formula has to be modified to take into account the boundary conditions. The zero-flux boundary conditions can be easily discretized by setting

$$f_{i,k+1/2} - g_{i,k+1/2} = 0, \quad i = 1, \ldots, N, \quad k = 0, M,$$

and we get

$$\frac{\mathrm{d}\boldsymbol{X}_1(t)}{\mathrm{d}t} = -\frac{1}{\Delta z}\boldsymbol{f}_{3/2} + \frac{1}{2\Delta z^2}\big(\boldsymbol{B}(\boldsymbol{X}_2) + \boldsymbol{B}(\boldsymbol{X}_1)\big)(\boldsymbol{X}_2 - \boldsymbol{X}_1), \tag{3.1}$$

$$\frac{\mathrm{d}\boldsymbol{X}_M(t)}{\mathrm{d}t} = \frac{1}{\Delta z}\boldsymbol{f}_{M-1/2} - \frac{1}{2\Delta z^2}\big(\boldsymbol{B}(\boldsymbol{X}_{M-1}) + \boldsymbol{B}(\boldsymbol{X}_M)\big)(\boldsymbol{X}_M - \boldsymbol{X}_{M-1}). \tag{3.2}$$

Let $\boldsymbol{\mathcal{X}} \in \mathbb{R}^{NM}$ be defined by $\boldsymbol{\mathcal{X}}^{\mathrm{T}} := (\boldsymbol{X}_1^{\mathrm{T}}, \ldots, \boldsymbol{X}_M^{\mathrm{T}})^{\mathrm{T}}$. One can rewrite this semi-discretization in a matrix/vector form as

$$\frac{\mathrm{d}\boldsymbol{\mathcal{X}}}{\mathrm{d}t} = -\frac{1}{\Delta z}(\Delta^- \boldsymbol{f})(\boldsymbol{\mathcal{X}}) + \frac{1}{\Delta z^2}\boldsymbol{\mathcal{B}}(\boldsymbol{\mathcal{X}})\boldsymbol{\mathcal{X}}, \tag{3.3}$$

where $\boldsymbol{\mathcal{B}}(\boldsymbol{\mathcal{X}})$ is an $(NM) \times (NM)$ block tridiagonal matrix whose blocks $\mathcal{B}_{ij}$ are N by N matrices generally given by

$$\mathcal{B}_{i,i}(\boldsymbol{\mathcal{X}}) = \frac{1}{2\Delta z^2}\big(\boldsymbol{B}(\boldsymbol{X}_{i+1}) + 2\boldsymbol{B}(\boldsymbol{X}_i) + \boldsymbol{B}(\boldsymbol{X}_{i-1})\big), \quad i = 2, \ldots, M-1,$$

$$\mathcal{B}_{i,i-1}(\boldsymbol{\mathcal{X}}) = B_{i-1,i}(\boldsymbol{\mathcal{X}}) = -\frac{1}{2\Delta z^2}\big(\boldsymbol{B}(\boldsymbol{X}_i) + \boldsymbol{B}(\boldsymbol{X}_{i-1})\big), \quad i = 2, \ldots, M,$$

with $\mathcal{B}_{1,1}(\boldsymbol{\mathcal{X}})$ and $\mathcal{B}_{M,M}(\boldsymbol{\mathcal{X}})$ properly defined taking into account the boundary condition discretizations (3.1)–(3.2).

3.2. **Time discretization.** For the time discretization we use the linearly implicit IMEX-RK scheme (LI-IMEX-RK) proposed in [4]. Linearly implicit methods were developed as an alternative to non-lineraly implicit IMEX-RK schemes (NI-IMEX-RK). In NI-IMEX-RK schemes the whole diffusive term $\boldsymbol{\mathcal{B}}(\boldsymbol{\mathcal{X}})\boldsymbol{\mathcal{X}}$ is treated implicitly requiring the resolution of at least one non-linear system of N by M scalar equations per time step. To solve those systems it is necessary to use a sophisticated solver for non-linear equations which can be really expensive in terms of computational time.

In LI-IMEX-RK schemes, the appearance of non-linear systems is avoided by considering the term $\boldsymbol{\mathcal{B}}(\boldsymbol{\mathcal{X}})$ in the product $\boldsymbol{\mathcal{B}}(\boldsymbol{\mathcal{X}})\boldsymbol{\mathcal{X}}$ as non-stiff while $\boldsymbol{\mathcal{X}}$ is considered stiff. The semi-discrete formulation (3.3) can then be written as

$$\frac{\mathrm{d}\boldsymbol{\mathcal{X}}}{\mathrm{d}t} = -\frac{1}{\Delta z}(\Delta^- \boldsymbol{f})(\boldsymbol{\mathcal{X}}^*) + \frac{1}{\Delta z^2}\boldsymbol{\mathcal{B}}(\boldsymbol{\mathcal{X}}^*)\boldsymbol{\mathcal{X}},$$

where $\boldsymbol{\mathcal{X}}^*$ is treated explicitly as an argument of $\boldsymbol{f}$ and $\boldsymbol{\mathcal{B}}$ while $\boldsymbol{\mathcal{X}}$ is implicit in the diffusive part.

The simplest first-order LI-IMEX-RK scheme for (3.3) is the one-step scheme that can be written as follows (this scheme will, however, not be used herein):

$$\boldsymbol{\mathcal{X}}^{n+1} = \boldsymbol{\mathcal{X}}^n - \frac{1}{\Delta z}(\Delta^- \boldsymbol{f})(\boldsymbol{\mathcal{X}}^n) + \frac{1}{\Delta z^2}\boldsymbol{\mathcal{B}}(\boldsymbol{\mathcal{X}}^n)\boldsymbol{\mathcal{X}}^{n+1}.$$

As it can be seen, the numerical solution can be obtained by solving a convection-diffusion equation with a linear diffusion term in which the matrix function $\boldsymbol{\mathcal{B}}$ is given.

4. Numerical examples

In all examples we assume that the transition concentration between discrete and hindered settling X_{trans} in (2.3) is set to a constant value $X_{\mathrm{trans}} = 1\,\mathrm{kg/m^3}$ and $v(X)$ is defined by (2.4) with

$r_{\mathrm{V}} = 0.45\,\mathrm{m}^3/\mathrm{kg}$ [36]. The solid and liquid densities are $\rho_X = 1050\,\mathrm{kg/m}^3$ and $\rho_L = 998\,\mathrm{kg/m}^3$ [6], respectively, and the acceleration of gravity is $g = 9.81\,\mathrm{m/s}^2$. The effective solids stress chosen is

$$\sigma_{\mathrm{e}}(X) = \begin{cases} 0 & \text{for } 0 \leq X \leq X_{\mathrm{crit}}, \\ \tilde{\alpha}(X - X_{\mathrm{crit}}) & \text{for } X > X_{\mathrm{crit}}, \end{cases}$$

where $\tilde{\alpha} = 0.5\,\mathrm{m}^2/\mathrm{s}^2$.

For the simulations we assume that the particle classes are ordered such that

$$0 < v_{0,1} < v_{0,2} < \cdots < v_{0,N},$$

and we assume that if $v_{0,i} < v_{0,j}$, then $X_{\mathrm{crit},i} < X_{\mathrm{crit},j}$, following the idea that faster settling particles would provide a denser packing before being subjected to the force of compression, due to their less porous structure [34]. Specifically, the individual critical concentrations are proposed to be

$$X_{\mathrm{crit},i} = X_{\mathrm{crit},1} + (i-1)\frac{X_{\mathrm{crit},N} - X_{\mathrm{crit},1}}{N-1}, \quad i = 2, \ldots, N-1,$$

where $X_{\mathrm{crit},1}$ is the critical concentration of the slowest class and hence the one with the smaller critical concentration, and $X_{\mathrm{crit},N}$ is the critical concentration of the fastest class, which has the largest critical concentration. Note that when $X_{\mathrm{crit},1} = X_{\mathrm{crit},N}$, then $X_{\mathrm{crit},i} = X_{\mathrm{crit},1}$ for $i = 2, \ldots, N-1$.

4.1. **Experiment 1.** To test the consistency of the multi-class model we compare the results obtained with the multi-class model with just one class present with the results obtained with the BD model. In Figure 3 we show the results obtained by both models using a mesh with $M = 100$ nodes. The critical concentration is set to $X_{\mathrm{crit}} = 6\,\mathrm{kg/m}^3$ while $X_{\mathrm{trans}} = 0$ since the BD model was designed only for the treatment of SST scenarios and does not acknowledge changes between discrete and hindered setlling. As can be seen in Figure 3 the results obtained by both models are very similar, even near discontinuities and the compression area, where the LI-IMEX-RK scheme results present smoother transitions.

To further test the consistency of the multi-class model we consider two suspensions: one with only a single class with initial concentration X_0 settling with velocity v and another one with the same total initial concentration as the first suspension but divided evenly between five classes, each one settling with velocity v (thus creating five identical classes). In this case the individual critical concentrations are $X_{\mathrm{crit},i} = 12\,\mathrm{kg/m}^3$ for $i = 1, \ldots, N$. As expected the sum of the concentrations of each class in the second suspension has the same settling behavior as the solids in the first suspension, as shown in Figure 4, proving the consistency of the multi-class model.

4.2. **Experiment 2.** In this experiment we apply the multi-class model to simulate discrete settling behaviour in a raw wastewater sample (as one would find in a PST). A batch experiment known as ViCAs [11] can be used to investigate this type of settling behaviour. A ViCAs experiment consists of a hanging column open at the bottom, where settled particles are captured as they exit the column. The mass of settled particles recovered at the bottom as a function of time provides a measure of the settling velocity distribution of the particles provided the total concentration is kept so low that only discrete settling occurs.

To simulate this experiment, we consider a homogeneous suspension with total initial concentration $X_0 = 0.1\,\mathrm{kg/m}^3 < X_{\mathrm{trans}} = 1\,\mathrm{kg/m}^3$ in a column of height 1 m, where $z = 0$ represents the top of the column and $z = 1$ represents its bottom. The suspension consists of 10 classes of particles with initial concentrations and velocities given by Table 1.

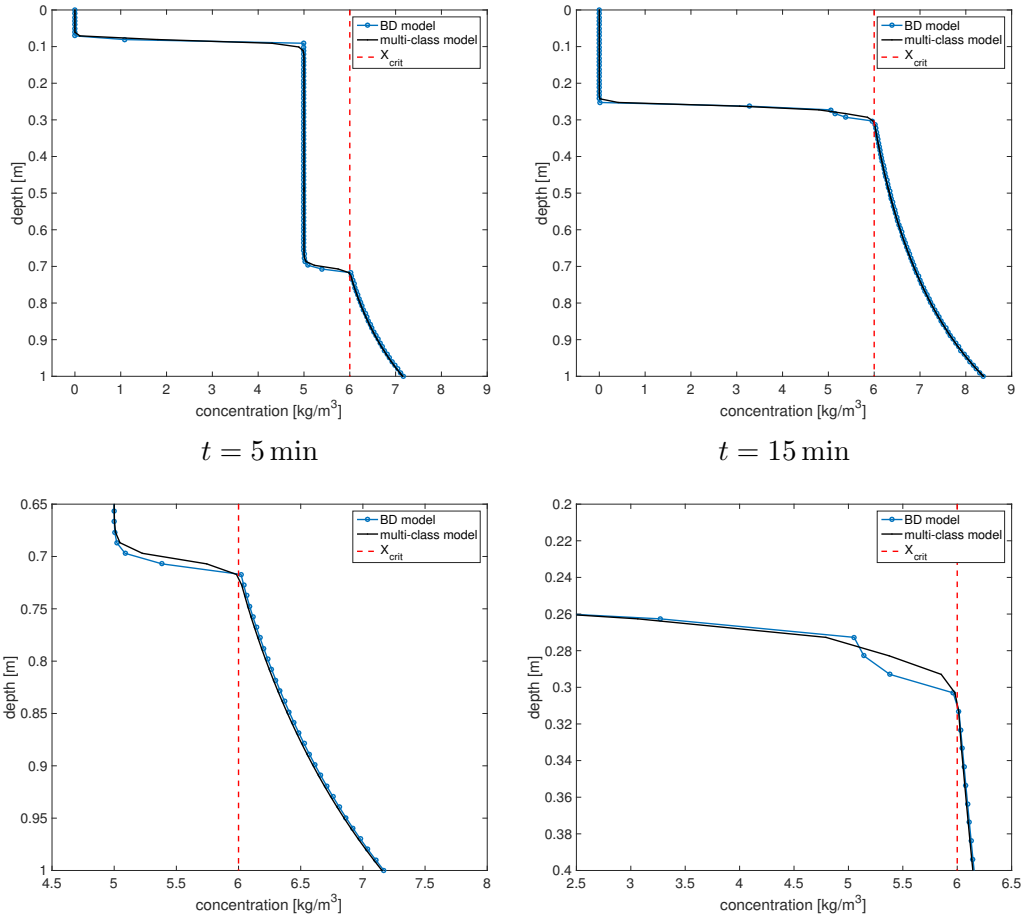

FIGURE 3. Experiment 1: simulated concentrations [kg/m^3] as function of normalized vessel depth. BD model and multi-class approximate solutions (top) and enlarged views (bottom) for times $t = 5$, 15 min.

Since $X_0 < X_{\text{trans}}$ and the solids are not accumulating at the bottom of the vessel, the total concentration will remain below the paramenter X_{trans} in all the domain. In this regime, where $X < X_{\text{trans}}$, the model is linear, and no interaction between classes takes place, so the structure forming between the bulk suspension at its initial composition and the supernatant clear liquid is a fan of 10 contact discontinuities, one per class, propagating downwards at speeds $v_{1,0} < v_{2,0} < \ldots < v_{10,0}$, where the discontinuity traveling at speed $v_{k,0}$ separates a region that is void of class k from a region in which class k is present at its initial concentration, as it can be seen in the concentration profiles displayed in Figure 5.

In this figure we can see the concentration profiles for times $t = 15\,\text{min}, 1\,\text{h}$ and $5\,\text{h}$ and the fraction of mass recovered from the vessel per class and per time step. As can be seen the different classes are removed sequentially from the column depending on their initial velocities and no hindrance is in effect. For example, while the tenth class, the fastest, has completely left the column after less than one minute, only 15% of the total mass of the slowest class has been removed from

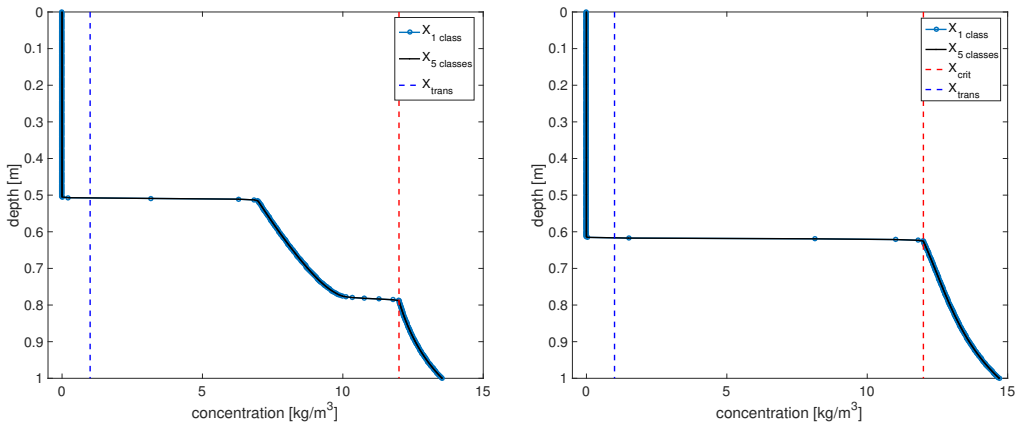

$t = 2\,\text{min}$ $t = 5\,\text{min}$

FIGURE 4. Experiment 1: comparison of the approximated solutions for the multi-class model between one and five classes satisfying $X_{1\text{class}} = \sum_{i=1}^{5} X_{5\text{classes},i}$.

	Experiment 2			Experiment 3	
i	$v_{0,i}$ [m/d]	$v_{0,i}$ [m/s]	$X_{0,i}$ [kg/m^3]	$v_{0,i}$ [m/d]	$v_{0,i}$ [m/s]
1	0.5	5.78×10^{-6}	0.021	5	5.78×10^{-5}
2	2	2.31×10^{-5}	0.003	20	2.31×10^{-4}
3	7	8.10×10^{-5}	0.005	70	8.10×10^{-4}
4	15	1.73×10^{-4}	0.01	150	1.73×10^{-3}
5	30	3.47×10^{-4}	0.011	300	3.47×10^{-3}
6	50	5.78×10^{-4}	0.01	500	5.78×10^{-3}
7	80	9.25×10^{-4}	0.0125	800	9.25×10^{-3}
8	130	1.50×10^{-3}	0.0085	1300	1.50×10^{-2}
9	200	2.31×10^{-3}	0.007	2000	2.31×10^{-2}
10	450	5.20×10^{-3}	0.012	4500	5.20×10^{-2}

TABLE 1. Initial concentrations $X_{0,i}$ and velocities $v_{0,i}$, in m/d and m/s, for Experiments 2 and 3.

the vessel after five hours of settling. Hence, this fraction will likely not be removed in full-scale PSTs where the typical residence time is approximately two hours.

In Figure 6 the simulated fraction of mass that is recovered from the vessel per time step is shown. It can be seen that a large part of the present particles is recovered early in the experiment (consisting of the faster settling classes and some slower settling particles present initially at the bottom of the column). Slower settling particle classes take much longer to reach the bottom of the column.

4.3. **Experiment 3.** In sharp contrast to PSTs where discrete settling is predominant, settling conditions in SSTs are such that all three settling regimes may occur simultaneously at different depths. This challenges the numerical method as transitions between different settling regimes may create sharp changes in the concentration and settling velocity profile. Therefore, in this third

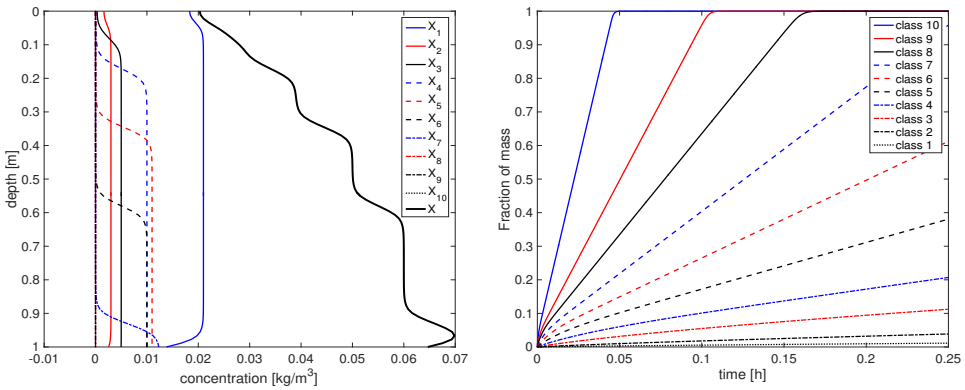

$t = 15\,\mathrm{min}$

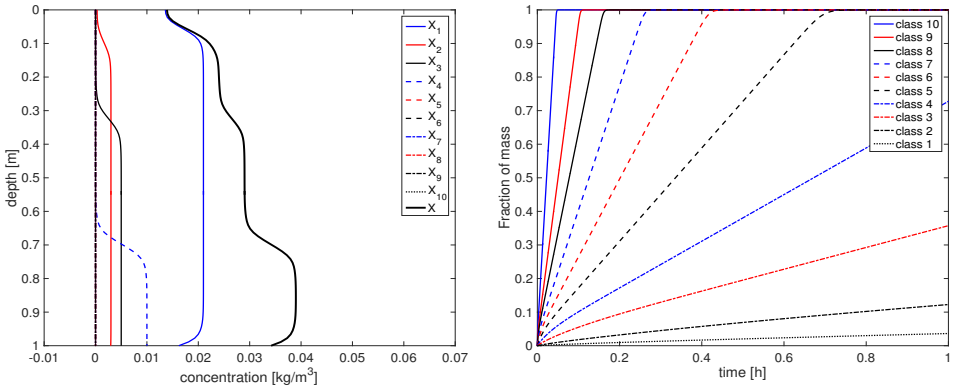

$t = 1\,\mathrm{h}$

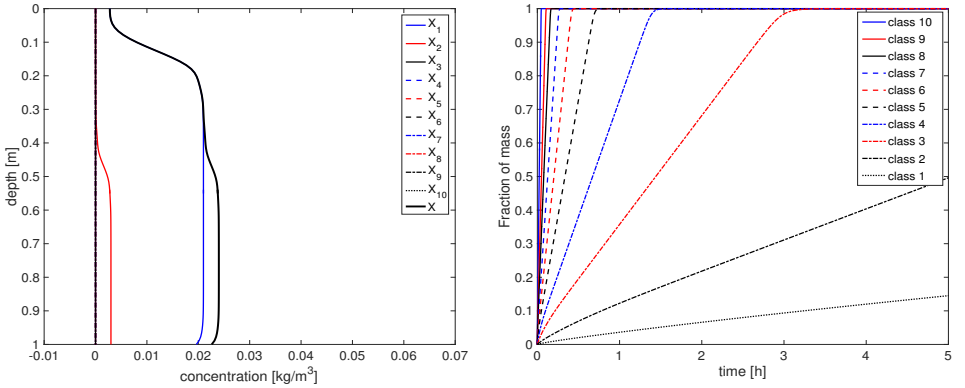

$t = 5\,\mathrm{h}$

FIGURE 5. Experiment 2: concentration of each class (left) and the fraction of initial mass per class that has left the vessel (right) at times $t = 15\,\mathrm{min}, 1\,\mathrm{h}, 5\,\mathrm{h}$.

experiment, we simulate batch settling of activated sludge. The settling suspension is again divided into 10 classes with initial velocities given by Table 1.

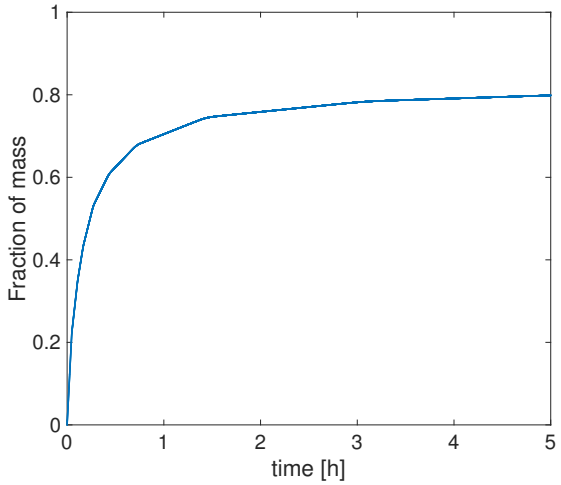

FIGURE 6. Experiment 2: fraction of mass that has left the vessel as a function of time.

Experiment 3a. In a first example, the total initial homogeneous concentration ($X_0 = 4\,\mathrm{kg/m^3}$) is equally distributed over the different classes, i.e $X_{0,i} = 0.4\,\mathrm{kg/m^3}$, $i = 1, \ldots, 10$, and the same critical concentration is considered for each class $X_{\mathrm{crit},i} = 12\,\mathrm{kg/m^3}$, $i = 1, \ldots, 10$.

Figures 7 and 8 show the concentration and velocity profiles for all classes throughout the settling column at different settling times. Faster particle classes can be seen to accumulate at the bottom early in the experiment, reaching the compression regime within $t = 1\,\mathrm{min}$. The discrete settling region is made up of only the slower settling classes since their settling velocities causes them to remain in the upper region where low concentrations prevail. In the hindered settling region particles of several classes are settling together which corresponds to the situation in which particles will be influencing each other's settling velocity. However, a slow segregation of particles of different classes can be observed causing the total concentration profile to decrease in a staircase fashion. This segregation is more pronounced as the total concentration decreases and particles become less hindered in their movement by surrounding particles. Moreover, upconcentration of specific classes can be observed at certain heights in the settling column. For example, at $t = 1\,\mathrm{min}$, the concentration of class 7 between $z = 0.2\,\mathrm{m}$ and $z = 0.3\,\mathrm{m}$ is increased compared to the concentration of this class below $z = 0.3\,\mathrm{m}$. This phenomenon was first observed experimentally by Smith [31] and is therefore sometimes called the "Smith effect" and is consistent with Corollary 3 of [35] that states that "when the fastest-settling species disappear, the concentration of each of the remaining species increases", see [9]. As class 8 is no longer present above $z = 0.3\,\mathrm{m}$, the total concentration decreases causing the remaining classes to be less hindered resulting in higher local settling velocities and an increase in concentration.

The same behavior is also reflected in the velocity distributions in Figure 8, where it can be seen that velocities are constant in the discrete area while they diminish and span a smaller range as particles start to hinder each other in the hindered regime. Finally, the settling velocities drop considerably when compression starts. The changes between settling regions are marked using dark dashed lines through all figures.

Experiment 3b. If we redefine the individual critical concentrations to vary linearly on a range between $X_{\mathrm{crit},1} = 8\,\mathrm{kg/m^3}$ and $X_{\mathrm{crit},10} = 14\,\mathrm{kg/m^3}$ (based on observations made in [14]), then some changes in the settling behavior of the system can be seen, especially in the compression area. In

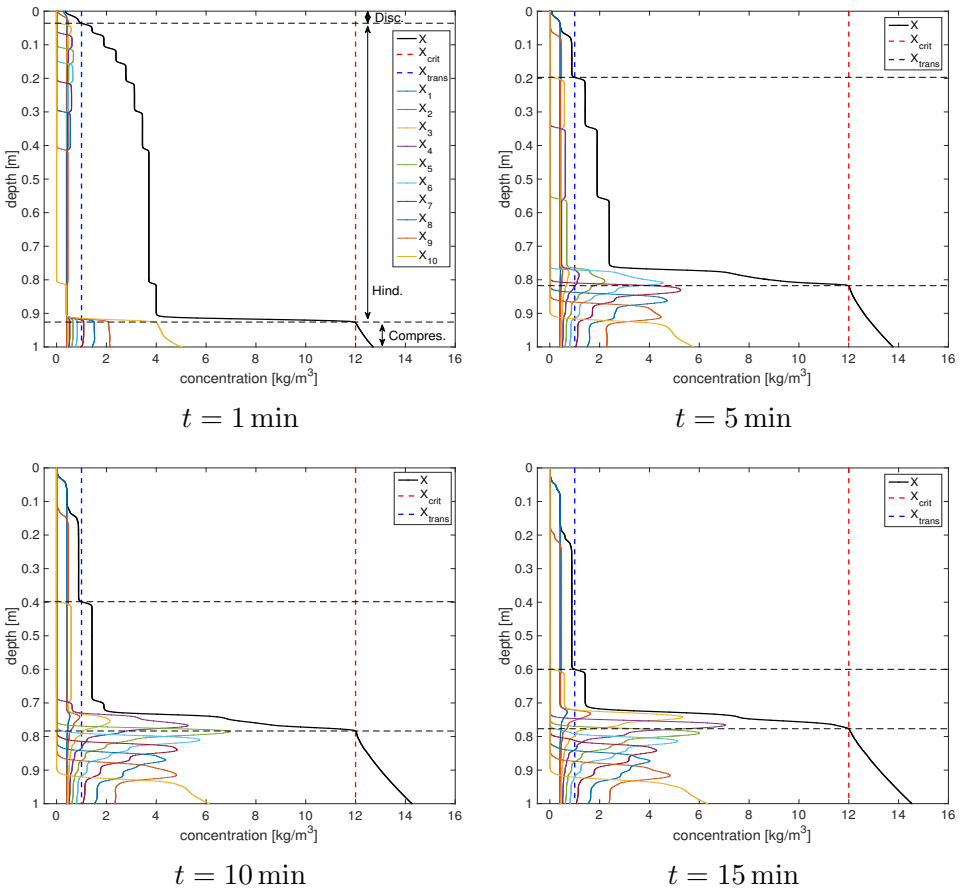

FIGURE 7. Experiment 3: temporal evolution of the concentration of each class using constant critical concentrations. The different settling regions are marked using black dashed lines.

Figure 9 we show the concentration profiles for times $t = 1, 5, 10, 15$ min. It can be seen how the function $\mathcal{X}_{\text{crit}}$ changes depending on the total concentration. In this case the compression region spans a wider concentration region and the sludge blanket shows a more gradual build-up than when using constant individual critical concentrations. Such more gradual build-up of the sludge blanket corresponds to experimental observations of De Clercq et al. [13].

Experiment 3c. Although the uniform initial distribution of total concentrations over the different classes allows us to test the behaviour of the model, it is not a distribution present in more realistic contexts. A normal or slightly skewed distribution would better represent typical wastewater or activated sludge samples. Changes in the initial homogeneous concentration distribution may produce different settling scenarios. We will therefore consider three different initial configurations with the same total initial concentration as before, $X_0 = 4\,\text{kg/m}^3$: a normally distributed initial concentration and a left- and a right-skewed initial distributions, see Figure 10. The velocity and individual critical concentration for each class are considered as before. The fact that the presented model is able to simulate differences in settling behaviour caused by changes in distribution and not solely by changes in concentration is one of the main features of the new framework. The

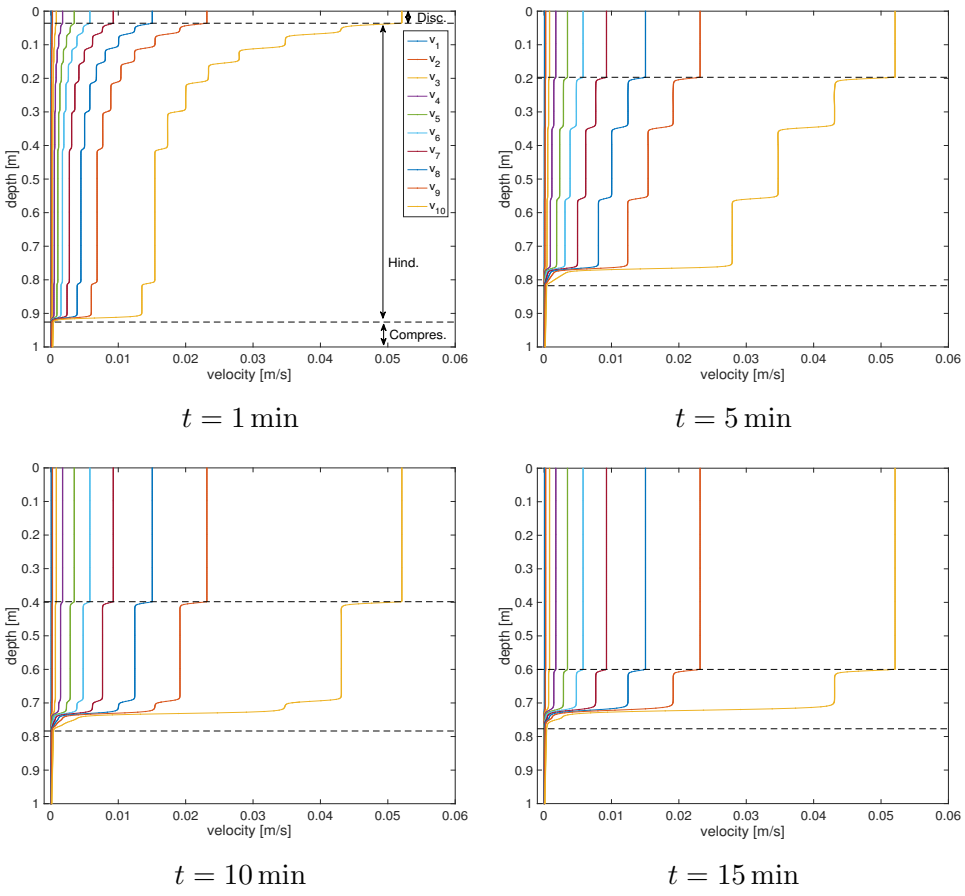

FIGURE 8. Experiment 3: temporal evolution of the velocity distribution for each class using constant critical concentration.

corresponding numerical method should thus be able to adequately handle such changes in initial particle distribution.

In Figure 11 we can see the concentration profiles obtained for times $t = 5$ and 15 min when considering the different initial concentration. As expected, the compression region develops faster when using a right-skewed initial concentration distribution as the faster classes have higher initial concentrations, while in the left-skewed distribution the settling is much slower. As a consequence, significant differences are observed in the predictions of sludge blanket height and bottom concentration. This is further illustrated in Figure 12 where the distribution of the particles through height and time is displayed for the left- and right-skewed distributions. Note that the line interpolating the nodes has only been drawn to better visualize the distribution of the particles.

Experiment 3d. Finally, to test the capabilities of the multi-class model for more extreme distributions we consider a right-skewed distribution for the concentrations with a peak in the first class, the one with the slowest particles, with a total initial concentration of $X_0 = 4\,\mathrm{kg/m^3}$. The initial velocities and individual critical concentrations are considered as in Experiment 3b. The definition of the concentration for each class can be seen in Figure 13 together with the temporal evolution

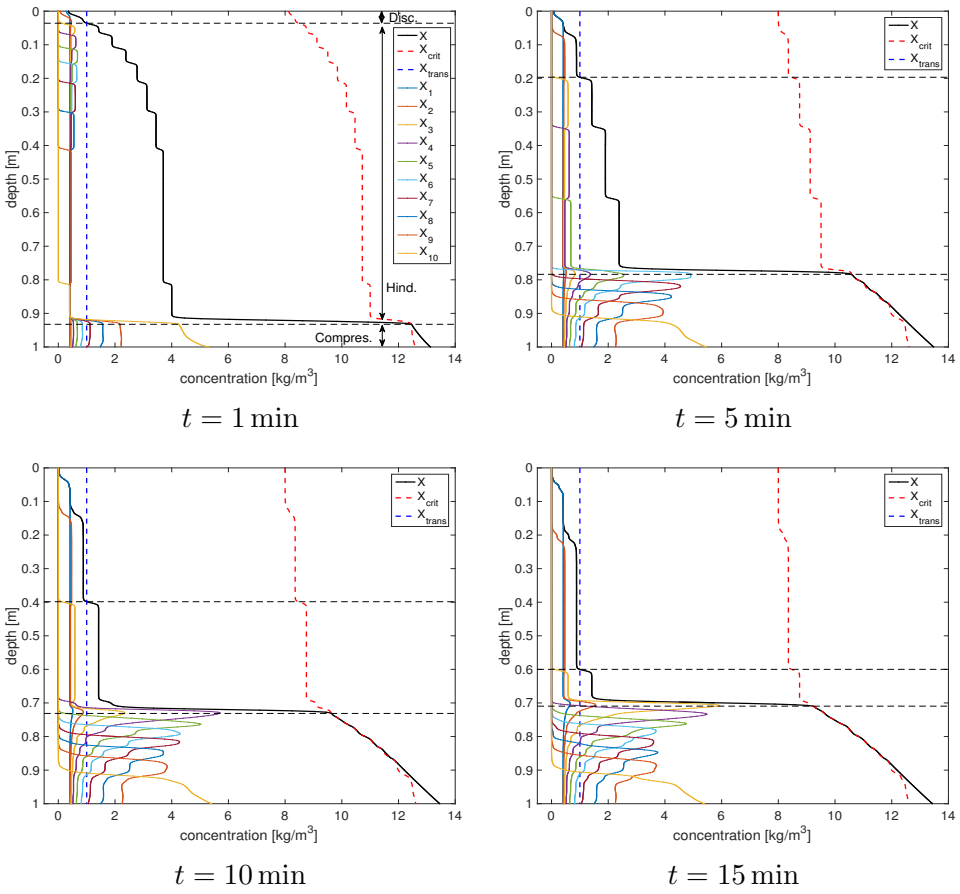

FIGURE 9. Experiment 3: temporal evolution of the concentration of each class using linerarly distributed critical concentrations.

of the concentrations. As is shown, we have a large amount of small particles moving really slow and thus remaining in the supernatant.

5. Conclusions

This article is part of an ongoing work to develop a consistent unified framework for the simulation of settling tanks in water resource recovery facilities.

We have shown the derivation of the model paying special attention to the application of multi-class to the definition of the critical concentration, giving an explicit representation of the critical manifold where a change of the character of the PDE system occurs, illustrated when two classes are considered. We have described in detail the numerical scheme applied to numerically solve the system of PDEs. Finally, in Section 4 we displayed a number of experiments that allow us to conclude that the proposed numerical technique is a reliable and robust tool for numerically solving our model. The results obtained with the multi-class model are comparable to those obtained by the state-of-the-art single class BD model and the results for both PST and SST simulation experiments seem physically correct and compatible with the results obtained for batch settling in laboratory experiments.

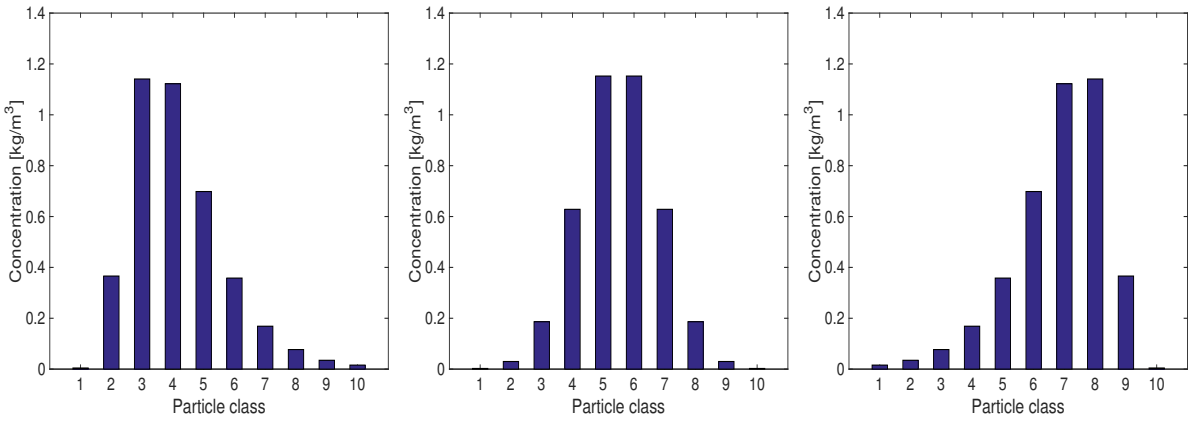

FIGURE 10. Experiment 3: initial distribution configurations.

While the numerical results essentially reconfirm that the model exhibits the expected solution behaviour, let us comment that the well-posedness and numerical analysis of strongly degenerate parabolic systems of PDEs such as (1.1) is a topic of current mathematical research.

ACKNOWLEDGEMENTS

R. Bürger is supported by Fondef project ID15I10291; CRHIAM, Proyecto Conicyt Fondap 15130015; Fondecyt project 1130154 and BASAL project CMM, Universidad de Chile and CI^{2}MA, Universidad de Concepción. M.C. Martí is supported by Conicyt Fondecyt/Postdoctorado/3150140. P. Vanrolleghem and E. Torfs are supported by the Natural Sciences an Engineering Research Council of Canada (NSERC/CRSNG), Veolia Water Technologies and Québec City. P. Vanrolleghem holds the Canada Research Chair on Water Quality Modelling. P. Mulet is supported by Ministerio de Economía y Competividad under grant MTM 2014-54388-P.

REFERENCES

[1] U. Ascher, S. Ruuth, J. Spiteri, Implicit-explicit Runge-Kutta methods for time dependent partial differential equations, Appl. Numer. Math., 25 (1997), 151–167.

[2] G. Bachis, T. Maruéjouls, S. Tik, Y. Amerlinck, H. Melcer, I. Nopens, P. Lessard, P.A. Vanrolleghem, Modelling and characterisation of primary settlers in view of whole plant and resource recovery modelling, Water Sci. Technol. 72 (2015) 2251–2261.

[3] S. Berres, R. Bürger, K.H. Karlsen, E.M. Tory, Strongly degenerate parabolic-hyperbolic systems modeling polydisperse sedimentation with compression, SIAM J. Appl. Math. 64 (2003) 41–80.

[4] S. Boscarino, R. Bürger, P. Mulet, G. Russo, L.M. Villada, Linearly implicit IMEX Runge-Kutta methods for a class of degenerate convection-diffusion problems, SIAM J. Sci. Comput. 37 (2015) B305–B331.

[5] S. Boscarino, R. Bürger, P. Mulet, G. Russo, L.M. Villada, On linearly implicit IMEX Runge-Kutta Methods for degenerate convection-diffusion problems modelling polydisperse sedimentation, Bull. Braz. Math. Soc. (N. S.) 47 (2016) 171–185.

[6] R. Bürger, S. Diehl, S. Farås, I. Nopens, E. Torfs, A consistent modelling methodology for secondary settling tanks: a reliable numerical method, Water Sci. Technol. 68 (2013) 192–208.

[7] R. Bürger, R. Donat, P. Mulet, C. A. Vega, On the implementation of WENO schemes for a class of polydisperse sedimentation models, J. Comput. Phys. 230 (2011) 2322–2344.

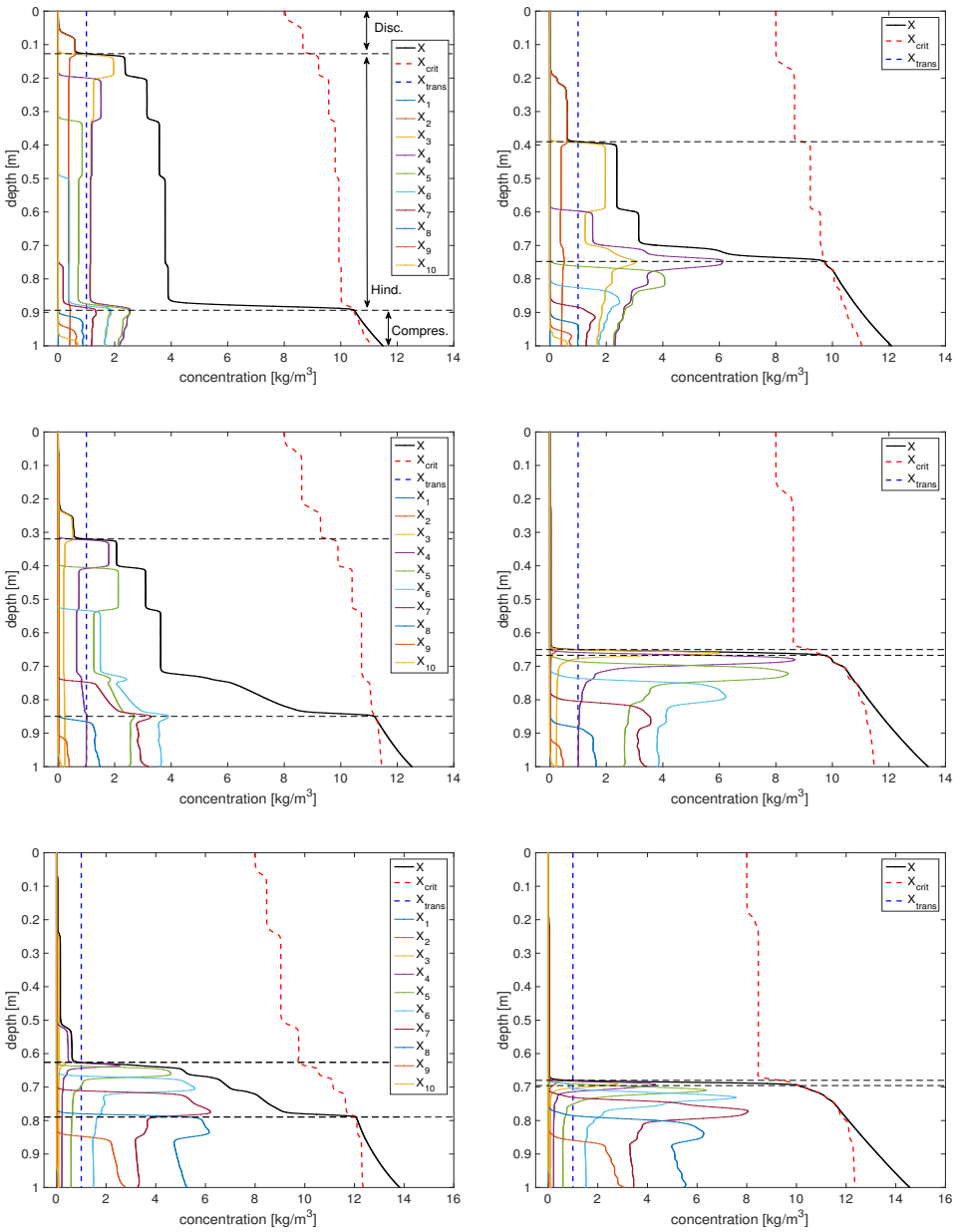

FIGURE 11. Experiment 3: temporal evolution of the concentration of each class from an initially left-skewed distribution of the concentrations (top), normal distribution (middle) and right-skewed distribution (bottom).

[8] R. Bürger, A. Kozakevicius, Adaptive multiresolution WENO schemes for multi-species kinematic flow models, J. Comput. Phys. 224 (2007) 1190–1222.

[9] R. Bürger, K.-K. Fjelde, K. Höfler, K.H. Karlsen, Central difference solutions of the kinematic model of settling of polydisperse suspensions and three-dimensional particle-scale simulations, J. Eng. Math. 41 (2001) 167–187.

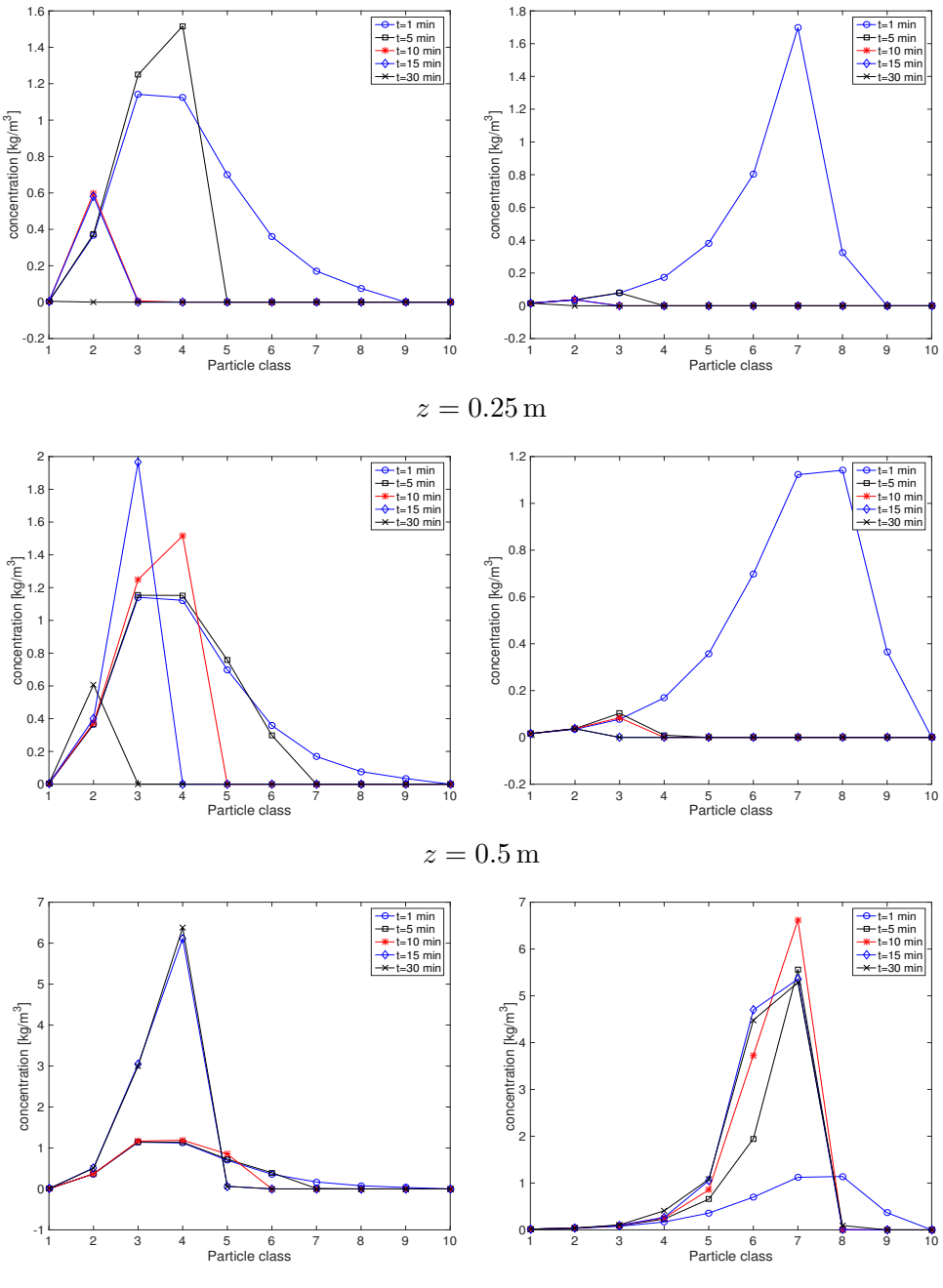

FIGURE 12. Experiment 3: particle distribution through time and height for the left- (left) and right- (right) biased normally distributed concentrations.

[10] R. Bürger, P. Mulet, L.M. Villada, Regularized nonlinear solvers for IMEX methods applied to diffusively corrected multi-species kinematic flow models, SIAM J. Sci. Comput. 35 (2013) B751–B777.

[11] G. Chebbo, M.-C. Gromaire, VICAS - An operating protocol to measure the distributions of suspended solid settling velocities within urban drainage samples, J. Environ. Eng. 135 (2009) 768–775.

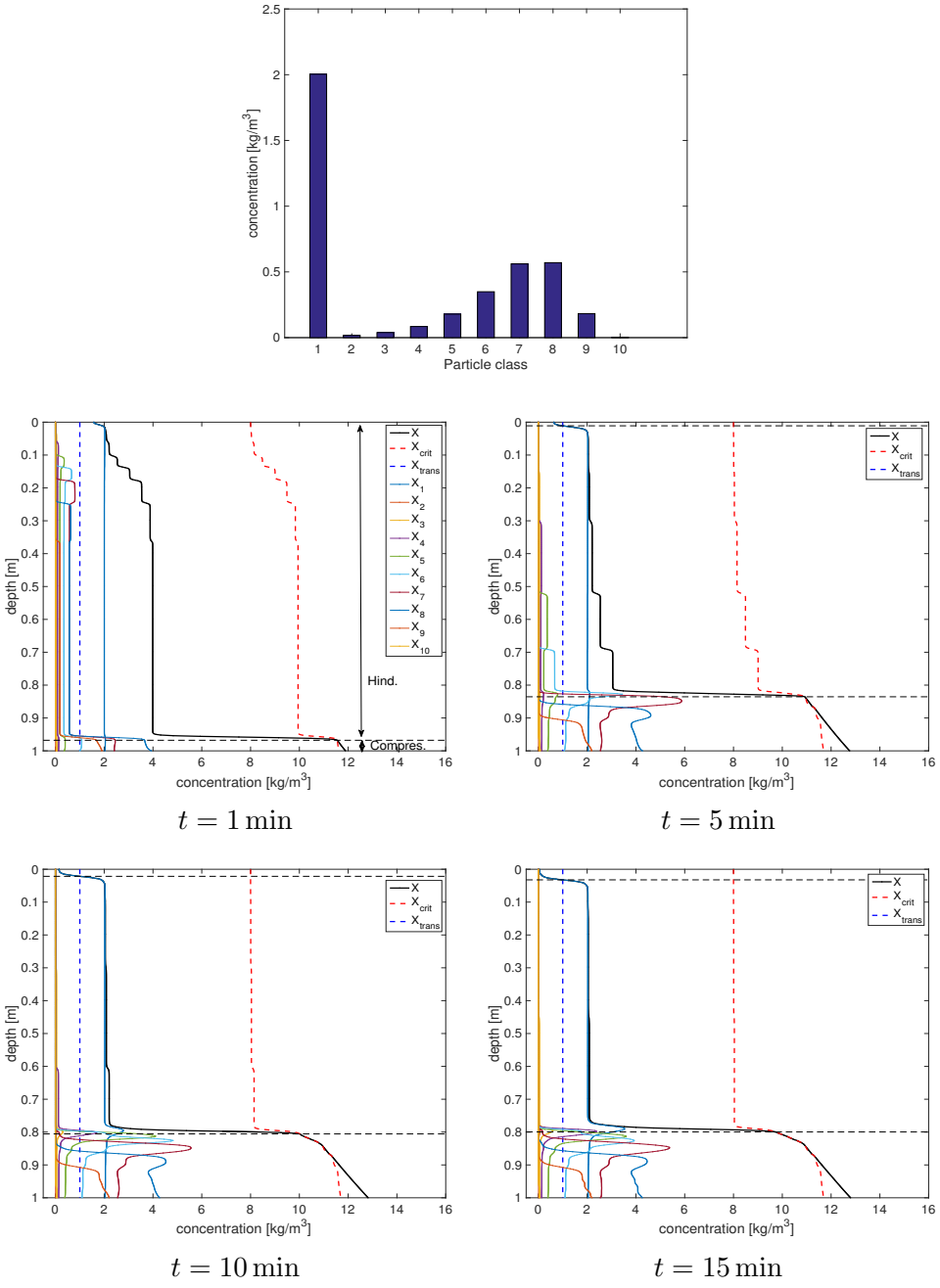

FIGURE 13. Experiment 3: temporal evolution of the concentration of each class using a right-skewed distribution for the initial concentrations except for a peak in the first class.

[12] G. Chiavassa, M.C. Martí, P. Mulet, Hybrid WENO schemes for polydisperse sedimentation models, Inter. J. Comput. Math. 93:11 (2016) 1801–1817.

[13] J. De Clercq, F. Jacobs, D.J. Kinnear, I. Nopens, R.A. Dierckx, J. Defrancq, P.A. Vanrolleghem, Detailed spatio-temporal solids concentration profiling during batch settling of activated sludge using a radiotracer, Water Res. 39 (2005) 2125–2135.
[14] J. De Clercq, I. Nopens, J. Defrancq, P.A. Vanrolleghem, Extending and calibrating a mechanistic hindered and compression settling model for activated sludge using in-depth batch experiments, Water Res. 42 (2008) 781–791.
[15] S. Diehl, Numerical identification of constitutive functions in scalar nonlinear convection-diffusion equations with application to batch sedimentation, Appl. Numer. Math. 95 (2015), 154–172.
[16] S. Diehl, S. Farås, G. Mauritsson, Fast reliable simulations of secondary settling tanks in wastewater treatment with semi-implicit time discretization, Comput. Math. Applic. 70 (2015) 459–477.
[17] R. Donat, F. Guerrero, P. Mulet, Implicit–explicit methods for models for vertical equilibrium multiphase flow, Comput. Math. Appl. 68 (2014) 363–383.
[18] R. Donat, P. Mulet, Characteristic-based schemes for multi-class Lighthill-Whitham-Richards traffic models, J. Sci. Comput. 37 (2008) 233–250.
[19] R. Donat, P. Mulet, A secular equation for the Jacobian matrix of certain multi-species kinematic flow models, Numer. Methods Partial Differ. Equ. 26 (2010) 159–175.
[20] G.A. Ekama, J.L. Barnard, F.W. Gunthert, P. Krebs, J.A. McCorquodale, D.S. Parker, E.J. Wahlberg, Secondary settling tank: theory, modelling, design and operation, IWA Scientific and Technical Report no. 6 (1997), IWA Publishing, London, UK.
[21] F. Guerrero, R. Donat, P. Mulet, Solving a model for 1-D, three-phase flow vertical equilibrium processes in a homogeneous porous medium by means of a Weighted Essentially Non-Oscillatory numerical scheme, Comput. Math. Appl. 66 (2013) 1284–1298.
[22] G.S. Jiang, C.-W. Shu, Efficient implementation of weighted ENO schemes, J. Comput. Phys. 126 (1996) 202–228.
[23] X.-D. Liu, S. Osher, T. Chan, Weighted essentially non-oscillatory schemes, J. Comput. Phys. 115 (1994) 200–212.
[24] M.C. Martí, P. Mulet, Some techniques for improving the resolution of finite difference component-wise WENO schemes for polydisperse sedimentation models, Appl. Numer. Math. 78 (2014) 1–13.
[25] R. Otterpohl, M. Freund, Dynamic models for clarifiers of activated sludge plants with dry and wet weather flows, Water Sci. Technol., 26(56) (1992), 1391–1400.
[26] B.G. Plósz, M. Weiss, C. Printemps, K. Essemiani, J. Meinhold, One-dimensional modelling of the secondary clarifier-factors affecting simulation in the clarification zone and the assessment of the thickening flow dependence, Water Res. 41 (2007) 3359–3371.
[27] E. Ramin, D. Wágner, L. Yde, P. Binning, M. Rasmussen, P. Mikkelsen, B. Plósz, A new settling velocity model to describe secondary sedimentation. Water Res. 66 (2014) 447–458.
[28] C.-W. Shu, Essentially non-oscillatory and weighted essentially non-oscillatory schemes for hyperbolic conservation laws, in Advanced Numerical Approximation of Nonlinear Hyperbolic Equations, Lecture Notes in Math. 1697, A. Quarteroni, ed., Springer-Verlag, Berlin, 1998 325–432.
[29] C.-W. Shu, S. Osher, Efficient implementation of essentially non-oscillatory shock-capturing schemes, J. Comput. Phys., 77(2) (1988) 439–471.
[30] C.-W. Shu, S. Osher, Efficient implementation of essentially non-oscillatory shock-capturing schemes, II. J. Comput. Phys., 83(1) (1989) 32–78.
[31] T.N. Smith, The sedimentation of particles having a dispersion of sizes, Trans. Instn. Chem. Engrs. (London) 44 (1966) T153–T157.
[32] I. Takács, G.G. Patry, D. Nolasco, A dynamic model for the clarification-thickening process, Water Res. 25 (1991) 1263–1271.
[33] S. Tik, G. Bachis, T. Maruéjouls, S. Charette, P. Lessard, P.A. Vanrolleghem, A CEPT model based on particle settling velocity distributions, Proceedings IWA Conference on Particle Separation 2016. Oslo, Norway, June 22–24 2016.
[34] E. Torfs, M.C Martí, F. Locatelli, S. Balemans, R. Bürger, S. Diehl, J. Laurent, P.A. Vanrolleghem, P. François, I. Nopens, Concentration-driven models revisited: Towards a unified framework to model settling tanks in WRRFs, Water Sci. Technol., DOI: 10.2166/wst.2016.485, in press.
[35] E.M. Tory and D. Pickard, Extensions and refinements of a Markov model of sedimentation, J. Math. Anal. Appl. 86 (1982) 442–470.
[36] P.A. Vesilind, Design of prototype thickeners from batch settling tests, Water Sew. Work. 115 (1968) 302–307.
[37] M. Zhang, C.-W. Shu, G.C.K. Wong, S.C. Wong, A weighted essentially non-oscillatory numerical scheme for a multi-class Lighthill-Whitham-Richards traffic flow model, J. Comput. Phys., 191 (2003) 639–659.

[38] M. Zhang, S.C. Wong, C.-W. Shu, A weighted essentially non-oscillatory numerical scheme for a multi-class traffic flow model on an inhomogeneous highway, J. Comput. Phys., 212 (2006) 739–756.

Centro de Investigación en Ingeniería Matemática (CI^{2}MA)

PRE-PUBLICACIONES 2016

2016-28 Luci Fatori, Tais De Olivera Saito, Mauricio Sepúlveda, Eiji Renan Takahashi: *Energy decay to Timoshenko system with indefinite damping*

2016-29 Sophie Balemans, Raimund Bürger, Stefan Diehl, Pierre Francois, Julien Laurent, Florent Locatelli, María Carmen Martí, Ingmar Nopens, Elena Torfs, Peter Vanrolleghem: *Concentration-driven models revisited: Towards a unified framework to model settling tanks in water resource recovery facilities*

2016-30 Ernesto Cáceres, Gabriel N. Gatica, Filander A. Sequeira: *A mixed virtual element method for the Brinkman problem*

2016-31 Ana Alonso-Rodriguez, Jessika Camaño, Rodolfo Rodríguez, Alberto Valli, Pablo Venegas: *Finite element approximation of the spectrum of the curl operator in a multiply-connected domain*

2016-32 David Mora, Gonzalo Rivera, Rodolfo Rodríguez: *A posteriori error estimates for a virtual elements method for the Steklov eigenvalue problem*

2016-33 Raimund Bürger, Gerardo Chowell, Elvis Gavilán, Pep Mulet, Luis M. Villada: *Numerical solution of a spatio-temporal gender-structured model for hantavirus infection in rodents*

2016-34 Felipe Lepe, Salim Meddahi, David Mora, Rodolfo Rodríguez: *Acoustic vibration problem for dissipative fluids*

2016-35 Alfredo Bermúdez, Marta Piñeiro, Rodolfo Rodríguez, Pilar Salgado: *Analysis of an ungauged T,\phi - \phi formulation of the eddy current problem with currents and voltage excitations*

2016-36 Jessika Camaño, Ricardo Oyarzúa, Ricardo Ruiz-Baier, Giordano Tierra: *Error analysis of an augmented mixed method for the Navier-Stokes problem with mixed boundary conditions*

2016-37 Eligio Colmenares, Gabriel N. Gatica, Ricardo Oyarzúa: *A posteriori error analysis of an augmented mixed-primal formulation for the stationary Boussinesq model*

2016-38 Rommel Bustinza, Ariel Lombardi, Manuel Solano: *An anisotropic a priori error estimate for a convection-dominated diffusion problem using the HDG method*

2016-39 Raimund Bürger, Stefan Diehl, María Carmen Martí, Pep Mulet, Ingmar Nopens, Elena Torfs, Peter Vanrolleghem: *Numerical solution of a multi-class model for batch settling in water resource recovery facilities*

Para obtener copias de las Pre-Publicaciones, escribir o llamar a: Director, Centro de Investigación en Ingeniería Matemática, Universidad de Concepción, Casilla 160-C, Concepción, Chile, Tel.: 41-2661324, o bien, visitar la página web del centro: `http://www.ci2ma.udec.cl`







Centro de Investigación en
Ingeniería Matemática (CI²MA)
Universidad de Concepción

Casilla 160-C, Concepción, Chile
Tel.: 56-41-2661324/2661554/2661316
http://www.ci2ma.udec.cl